Targeting CMTM6 Suppresses Stem Cell–Like Properties and Enhances Antitumor Immunity in Head and Neck Squamous Cell Carcinoma

Lei Chen[1], Qi-Chao Yang[1], Yi-Cun Li[1], Lei-Lei Yang[1], Jian-Feng Liu[1], Hao Li[1], Yao Xiao[1], Lin-Lin Bu[1], Wen-Feng Zhang[1,2], and Zhi-Jun Sun[1,2]

ABSTRACT

CMTM6, a regulator of PD-L1 expression, also modulates tumor immunity. Little is known about the function of CMTM6 and its mechanism of action in head and neck squamous cell carcinoma (HNSCC). In this study, we found by IHC analysis that CMTM6 overexpression predicted a poor prognosis for patients with HNSCC. We discovered that CMTM6 expression was correlated with increased activity through the Wnt/β-catenin signaling pathway, which is essential for tumorigenesis, maintenance of cancer stem cells (CSC), and the epithelial-to-mesenchymal transition (EMT) characteristic of multiple cancers. We used short hairpin RNA to eliminate expression of CMTM6, which led, in HNSCC cells, to reduced expression of nuclear β-catenin as well as inhibition of stem cell–like properties, TGFβ-induced EMT, and cell proliferation. Consistent with these results, we identified a significant positive correlation between expression of *CMTM6* and EMT- and CSC-related genes in The Cancer Genome Atlas (TCGA). We found positive correlations for both RNA and protein between expression of CMTM6 and immune checkpoint components. CMTM6 silencing–induced PD-L1 downregulation delayed SCC7 tumor growth and increased $CD8^+$ and $CD4^+$ T-cell infiltration. The proportions of PD-1^+, TIM-3^+, VISTA$^+$, LAG-3^+, and B7-H3^+ exhausted T cells were decreased significantly in the CMTM6 knockdown group. CMTM6 thus regulates stemness, EMT, and T-cell dysfunction and may be a promising therapeutic target in the treatment of HNSCC.

Introduction

Head and neck squamous cell carcinoma (HNSCC), a heterogeneous epithelial tumor, is the sixth most common malignancy and affects approximately 600,000 patients per year worldwide, with a mortality of 40%–50% (1, 2). Alcohol, betel quid, and tobacco exposure are the major causes of HNSCC (3, 4). Human papillomavirus (HPV) infection is an independent risk factor for oropharyngeal tumors, which occur primarily in the Western world (4, 5). The 5-year survival rate of HNSCC has not improved over the past three decades, despite improvements in therapeutics (6). The low survival rate is mainly due to recurrence and metastases (3). A better understanding of the molecular mechanisms of tumorigenesis is needed for understanding HNSCC.

Wnt/β-catenin signaling in HNSCC is involved in a variety of processes, such as proliferation, cancer cell stemness, and differentiation with mesenchymal traits (7, 8). With the epithelial-to-mesenchymal transition (EMT), cells lose epithelial characteristics and acquire mesenchymal features to gain mobility. EMT is crucial for tumor metastasis (9). EMT is driven by EMT-activating transcription factors (EMT-TF, including the SNAIL, TWIST, and ZEB families; ref. 10). The activation of EMT-TFs in cancer cells is associated with the maintenance of stemness properties (11), which links EMT to the concept of cancer stem cells (CSC). During EMT, cancer cells may resemble CSCs and exhibit enhanced self-renewal, metastasis, and drug resistance capabilities (11), characteristics evident in HNSCC (12). EMT may allow cancer cells to escape immune surveillance by various mechanisms (13). Similarly, CSCs have a negative impact on the effectiveness of immunotherapy (14). PD-L1, an immune inhibitory receptor with functions in cancer immune evasion, regulates EMT, the CSC-like phenotype, metastasis, and chemotherapy resistance (15). These findings suggest potential links among CSCs, EMT characteristics, and tumor immunity, although what those linkages are in the context of HNSCC remains unknown.

CMTM6 belongs to the CKLF-like MARVEL transmembrane domain–containing family (CMTM1–8) and is expressed at the plasma membrane of various cells (16). CMTM6 stabilizes PD-L1 protein expression to impair T-cell function (17, 18). CMTM6 increases PD-L1 expression without compromising antigen presentation by reducing MHC class I expression. Thus, the depletion of CMTM6 in cancer cells could enhance tumor-specific T-cell activity. CMTM6 synergizes with other immune checkpoint molecules, such as TIM-3 and B7-H3 (19). Elevated CMTM6 in gastric cancer is associated with a poor prognosis (19), and CMTM6 expression in combination with PD-L1 expression is a prognostic indicator in triple-negative breast cancer and pancreatic ductal adenocarcinoma (20). These findings suggest that CMTM6 may be a useful therapeutic target.

In this study, we found that, in HNSCC, CMTM6 is overexpressed and may be a prognostic IHC biomarker. Genetic ablation of CMTM6 reduces PD-L1 expression and restrains HNSCC cell proliferation. CMTM6 expression is correlated with Wnt/β-catenin signaling. *In vitro* depletion of CMTM6 affects the maintenance of stemness properties and inhibits TGFβ-induced EMT in HNSCC cells. We also observed a positive association between expression of CMTM6 and immune checkpoints. In an allograft mouse model, the

[1]The State Key Laboratory Breeding Base of Basic Science of Stomatology (Hubei-MOST) and Key Laboratory of Oral Biomedicine, Ministry of Education, School and Hospital of Stomatology, Wuhan University, Wuhan, China. [2]Department of Oral Maxillofacial-Head Neck Oncology, School and Hospital of Stomatology, Wuhan University, Wuhan, China.

Note: Supplementary data for this article are available at Cancer Immunology Research Online (http://cancerimmunolres.aacrjournals.org/).

Corresponding Author: Zhi-Jun Sun, School and Hospital of Stomatology, Wuhan University, Wuhan 430079, China. Phone: 8627-8768-6108; Fax: 8627-8787-3260; E-mail: sunzj@whu.edu.cn

Cancer Immunol Res 2020;8:179–91

doi: 10.1158/2326-6066.CIR-19-0394

immunosuppressed tumor state was relieved and tumor growth was inhibited in the CMTM6 knockout group compared with the control group. We conclude that CMTM6 participates in the regulation of CSCs and EMT phenotypes in HNSCC cells and that targeting CMTM6 may be an alternative strategy for HNSCC treatment.

Materials and Methods

Antibodies

Primary antibodies for IHC, immunofluorescence, and immunoblotting: anti-CMTM6 (HPA026980) was obtained from Sigma-Aldrich. Anti-PD-L1 (#13684, #29122 and #64988), anti-β-Catenin (#8480), anti-CD44 (#3570), anti-ALDH1A1 (#36671), anti-BMI1 (#6964), anti-Vimentin (#5741), anti-E-Cadherin (#3195), anti-N-Cadherin (#13116), anti-VISTA (#54979), anti-B7-H3 (#14058), anti-B7-H4 (#14572), anti-TIM-3 (#45208), anti-CD8α (#98941), anti-Histone H3 (#4499), and anti IgG (#3900S) were all from Cell Signaling Technology. Anti-LAG-3 (ab209236) was from Abcam, anti-CD4 (GB11064) was from Servicebio, and anti-CMTM6 (GTX108450) was obtained from GeneTex.

Flow cytometry

FITC anti-human PD-L1 (393605), APC anti-mouse PD-L1 (124312), PerCP/Cyanine5.5 anti-mouse CD8a (100733), PE anti-mouse B7-H3 (124507), PE anti-mouse VISTA (150203), APC anti-mouse B7-H4 (139407), and APC anti-mouse TIM-3 (134007) were purchased from BioLegend and eFluor 450 anti-mouse CD4 (48-0041-80), PE anti-mouse PD-1 (12-9985-81), PE anti-mouse LAG-3 (12-2231-81), eFluor 506 Fixable Viability Dye (65-0866-14) were from eBioscience. APC-Cyanine7 anti-mouse CD45 (561037) and FITC anti-mouse CD3 (561798) were obtained from BD Pharmingen.

Human HNSCC tissues

All human studies were approved by the Medical Ethics Committee of the Hospital of Stomatology, Wuhan University (Wuhan, China; 2016LUNSHENZI62). In this study, we used three sets of HNSCC tissue microarrays, derived from 210 cases of primary HNSCC, 69 cases of oral epithelial dysplasia, and 42 cases of normal oral mucosae. All tissue specimens were collected from the School and Hospital of Stomatology, Wuhan University (Wuhan, China) from 2011 to 2016, and all patients who provided a specimen signed informed consent under an approved institutional guideline. HNSCC specimens were clinically and pathologically graded according to the guidelines of the Union for International Cancer Control (UICC 2002) and the World Health Organization grading scheme, respectively.

Cell culture and treatment

The human HNSCC cell lines SCC4, SCC9, SCC15, and SCC25 (all from ATCC, 2014–2019) were maintained in F12/DMEM with 400 ng/mL hydrocortisone. CAL27 (obtained from ATCC, 2014) was cultured in DMEM/high glucose. The mouse HNSCC cell line SCC7 (obtained from Otwo Biotech, 2019) was cultured in RPMI1640 medium. Ten percent FBS (Gibco) and 1% penicillin/streptomycin were added to the above medium. The primary oral keratinocyte cell line (OKC) was cultured in serum-free keratinocyte medium (Gibco). Short tandem repeat authentication was performed for CAL27 and SCC4 in the experiment, but other cells have not been authenticated in the past year. All cell lines were used exclusively between passages 3 and 8 and were tested annually for *Mycoplasma* contamination by PCR (TransDetect). For the TGFβ-induced EMT assay, cells were treated with 8 ng/mL recombinant human TGFβ1 (PeproTech) for 1, 3, and 5 days. For the *in vitro* induction of PD-L1, SCC7 cells were treated with recombinant murine IFNγ (10 ng/mL, PeproTech) for 24 hours.

Cell proliferation and colony formation assays

For the cell proliferation assay, human HNSCC cell lines SCC4 or CAL27 were inoculated into 96-well flat-bottom plates (Corning) at 2,000 cells per well in the corresponding medium supplemented with 10% FBS. At 24, 48, and 72 hours, 20 μL CCK8 reagent (Dojindo) was added to each well, and the plates were incubated at 37°C for 2 hours. The absorbance was then measured at 450 nm using a BioTek plate reader (BioTek).

For the colony formation assay, 500 SCC4 or CAL27 cells were added to each well in a 6-well flat-bottomed plate in the corresponding medium supplemented with 10% FBS. After 10 days of culture, the cells were fixed using 4% paraformaldehyde and stained using crystal violet. The number of colonies was counted by ImageJ.

Sphere assay

Human HNSCC cell lines CAL27 (5,000 per plate) were cultured on 6-well Ultra-Low Attachment Microplates (Costar, Corning) in sphere medium [DMEM/F12 + N2 supplement (1%, R&D Systems) + B27 (1%, Gibco) + bFGF (20 ng/mL, Invitrogen) + EGF (20 ng/mL, Gibco)]. Ten days later, spheres larger than 100 μm in diameter were counted. Sphere formation ratios were calculated as sphere number divided by 5,000.

Flow cytometry

Monolayer HNSCC and primary OKC cells were washed with PBS after trypsin digestion, and single-cell suspensions were stained with a cell surface PD-L1 antibody for 1 hour in PBS (2% FBS) at 4°C after Fc blocking. Samples were run on a flow cytometer (CytoFLEX S, Beckman Coulter), and data were analyzed by FlowJo 10 (V10.0.6, Tree Star). For mouse tumor-infiltrating lymphocyte (TIL) staining, tumor samples were digested in RPMI1640 medium with collagenase D (1 mg/mL, Roche), hyaluronidase (0.1 mg/mL, Biosharp), and DNase I (0.2 mg/mL, BioFroxx) at 37°C for 30 minutes after dissociation (gentleMACS Dissociator, Miltenyi Biotec). Then, the cells were filtered through a 70-μm strainer. The lymphocytes were separated with Lymphoprep (StemCell Technologies) according to the manufacturer's protocol. The cell staining and detection methods were the same as described above.

The ALDEFLUOR Kit (StemCell Technologies) was used to analyze aldehyde dehydrogenase (ALDH) enzyme activity. A total of 10^6 cells/mL (CAL27 or SCC4) in ALDEFLUOR Assay Buffer were incubated with ALDEFLUOR reagent for 40 minutes at 37°C, and diethylaminobenzaldehyde was added to each sample as a negative control. The samples were analyzed on a CytoFLEX S, and data were analyzed in CytExpert.

Western blotting

Whole-cell extracts of cultured cells or sphere cells were lysed using M-PER Protein Extraction Reagent (containing protease and phosphatase inhibitors, Thermo Fisher Scientific). Nuclear proteins were extracted using a nucleoprotein extraction kit (Beyotime). For immunoblotting, the proteins were denatured by boiling, separated by 8%–10% SDS-PAGE, and transferred onto polyvinylidene difluoride membranes (Roche). After blocking with nonfat milk (5%) for 1 hour at room temperature, the blots were incubated overnight with the indicated antibodies at 4°C and were incubated with horseradish peroxidase–conjugated secondary antibodies (Biosharp) for 1 hour at room temperature on the subsequent day. Finally, the blots were

detected with an ECL kit (Advansta), and images were visualized and quantified using the Odyssey System (LI-COR Biosciences).

Generation of knockout cell lines

The short hairpin RNA (shRNA) targeting sequences specific for the human and mouse CMTM6 were as follows: shCMTM6-1 (human): 5′-AGGTCAAGAAGGCAGTTTT-3′; shCMTM6-2 (human): 5′ CCCAAGACAGTGAAAGTAA-3′; shCMTM6 (mouse): 5′-TGCC-TAACAGAAAGCGTGT-3′. shCtrl: 5′-GGGTATCGACGATTAC-AAA-3′ (18). A PLKO.1 vector encoding shRNA for a negative control (Sigma-Aldrich) or a CMTM6 target molecule was transfected into HEK293T cells together with psPAX2 and pMD2.G with Lipofectamine 2000 (Sigma-Aldrich). The culture lentiviral supernatant was harvested 48 hours after transfection. HNSCC cells were infected with the supernatants in the presence of 8 μg/mL polybrene (Sigma-Aldrich). Twenty-four hours after transduction, the cells were selected by 4 μg/mL puromycin (Sigma-Aldrich).

IHC and quantification

The 4-μm paraffin-embedded tissue sections were deparaffinized, rehydrated in xylene and an alcohol gradient, and heated in a sodium citrate solution for antigen retrieval. After endogenous peroxidase activity (3% hydrogen peroxide, 20 minutes) and nonspecific binding (goat or donkey serum, 30 minutes) were blocked, the sections were incubated overnight with the indicated antibodies at 4°C in a humidified box, and then incubated with the secondary biotinylated IgG antibody and an avidin–biotin–peroxidase reagent on the subsequent day. Finally, DAB reagent (Mxb Biotechnologies) was used to detect these labeled antibodies, and the nucleus was stained with hematoxylin. Primary antibodies were replaced with IgG as a negative control (Supplementary Fig. S1A). All slides were scanned by an Aperio ScanScope CS scanner (Aperio) with background subtraction. Aperio ImageScope software (V11.1.2) was used for membrane, nuclear, or pixel quantification. The cancer or mucosal region of interest was selected for quantitative analysis. The histoscore of membrane and nuclear staining was calculated as a percentage of positive cells using the formula (total intensity of strong positive) × 3 plus (total intensity of positive) × 2 plus (total intensity of weak positive) × 1. The histoscore of pixel quantification was calculated as the total intensity/total cell number. The threshold for scanning positive cells was set according to the standard controls provided by Aperio (21).

Immunofluorescence

HNSCC cells were cultured in 10-mm laser confocal dishes (NEST Biotechnology) with medium containing 10% FBS for 24 hours, fixed with 4% paraformaldehyde for 15 minutes, permeabilized with 0.5% Triton X-100 in PBS for 10 minutes at room temperature, and blocked with 5% BSA for 1 hour at 37°C. The cells were incubated overnight with the indicated antibodies at 4°C and then with the corresponding fluorescence-conjugated secondary antibody (Abbkine) for 1 hour at room temperature. Antifade Fluorescence Mounting Medium with DAPI (ZSGB-BIO) was used to mount the slides, and images were taken with a confocal microscope (FV1200, Olympus Life Science). For tumor sphere immunofluorescence, microspheres were collected in centrifuge tubes and then stained as described above; images were obtained by confocal microscopy with z-axis scanning.

ELISA

Tumor homogenates (100 mg tissue/mL PBS) were centrifuged for 20 minutes at 3,000 rpm, supernatants were collected, and protein concentrations were normalized by a BCA Protein Kit (Beyotime). IFNγ, Granzyme B, and TNFα concentrations in the supernatants were detected by commercial ELISA kits (4A Biotech) according to the manufacturer's instructions.

Animal experiments

Five-week-old female C3H/HeNCr MTV (C3H) mice were purchased from Charles River Laboratories. Then, 2×10^5 SCC7 cells (WT, shCMTM6, or shCtrl) were subcutaneously injected into C3H mice. The tumor volume was calculated as $1/2 \times \text{length} \times \text{width}^2$. All mice were sacrificed on day 20 after inoculation, and tumor samples were dissected and immediately preserved.

For *in vivo* $CD8^+$ T-cell depletion, SCC7 tumor–bearing mice were treated intraperitoneally (i.p.) with anti-mouse CD8 (250 mg; BE0004-1; BioXCell) on days −1, 1, 4, and 8. We verified the efficacy of $CD8^+$ T-cell depletion by flow cytometry (Supplementary Fig. S1B). All animal studies were approved and supervised by the Animal Care and Use Committee of Wuhan University (Wuhan, China).

Statistical analyses

All statistical analyses were performed with GraphPad Prism 7 software (GraphPad Software). Comparisons between groups of continuous variables were performed using two-tailed unpaired Student *t* tests (2 groups) or one-way ANOVA tests (> 2 groups). Correlations were determined by Pearson and Spearman *r* coefficient. Error bars shown in the data are presented as the means ± SD, and $P < 0.05$ was considered statistically significant.

Results

CMTM6 overexpression in HNSCC is associated with a poor prognosis

To gain insight into the role of CMTM6 in HNSCC progression, we detected CMTM6 expression by IHC analysis in custom-made HNSCC tissue microarrays (**Fig. 1A**). CMTM6 expression was significantly elevated in tumor tissues ($n = 210$) compared with normal mucosal ($n = 42$, $P < 0.001$) and dysplasia tissues ($n = 69$, $P < 0.01$; **Fig. 1A** and **B**). Specifically, CMTM6 was predominantly localized at the membrane of tumor cells, with some localization in the cytoplasm, and its expression was very similar to that of PD-L1 (http://www.proteinatlas.org/ENSG00000120217-CD274/pathology). We next examined the relationships of CMTM6 expression with clinicopathologic parameters and patient survival. The results indicated that patients with HNSCC with a high pathologic grade (II and III) displayed higher CMTM6 expression than those with a low pathologic grade (I; **Fig. 1A** and **C**). Consistently, analysis of the HNSCC cohort in The Cancer Genome Atlas (TCGA) by UALCAN (22) showed that *CMTM6* RNA expression was increased in patients with a higher pathologic grade (**Fig. 1D**). Furthermore, CMTM6 expression had a positive correlation with positive lymph node status, and tumor tissues from patients with lymph node metastasis stained more strongly [N(−) vs. N(+), $P < 0.01$; **Fig. 1E** and **F**]. Next, we examined the prognostic value of CMTM6 expression in HNSCC. Kaplan–Meier analysis with the log-rank test showed that patients with higher CMTM6 expression had poorer outcomes, and vice versa [best cutoff (23) = 95.05, $P = 0.0019$, **Fig. 1G**; median cutoff = 179.91, $P = 0.1283$, Supplementary Fig. S1C]. However, CMTM6 expression was independent of tumor size (T1–T4), TPF chemotherapy, HPV status, and smoking or alcohol consumption. In addition, CMTM6 expression levels were not significantly altered in metastatic lymph nodes and HNSCC tissues from patients who underwent preoperative radiotherapy treatment or presented with recurrence

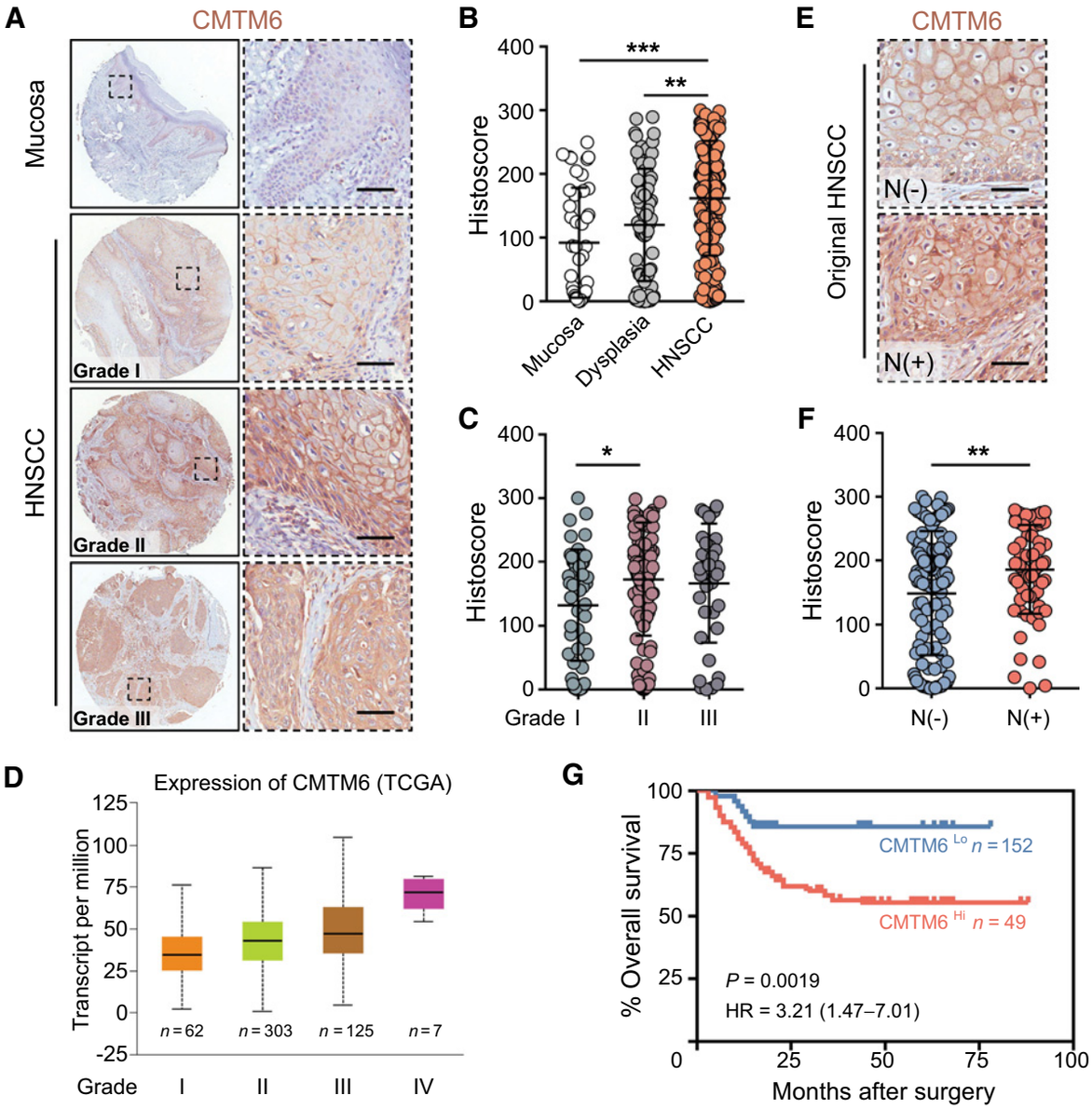

Figure 1.

CMTM6 is overexpressed and predicts a poor prognosis for patients with HNSCC. **A,** Representative IHC staining images of CMTM6 in normal mucosa and HNSCC tissues with different clinical pathologic grades (scale bar, 50 μm). **B,** Expression of CMTM6 protein in human HNSCC ($n = 210$) was higher than in oral mucosa ($n = 42$) and dysplasia ($n = 69$) by IHC analysis (**, $P < 0.01$; ***, $P < 0.001$). **C,** Quantification analysis of CMTM6 staining in HNSCC with different grades (I, $n = 53$; II, $n = 121$; III, $n = 36$; *, $P < 0.05$). **D,** Boxplot indicating *CMTM6* expression in different grades of HNSCC from the UALCAN database (***, $P < 0.001$ for I vs. III, I vs. IV, and II vs. IV; **, $P < 0.01$ for II vs. III and III vs. IV). Representative IHC staining of CMTM6 in metastasis-free (top, $n = 138$) and metastatic HNSCC tissue (**E**; bottom, $n = 72$; scale bar, 50 μm) and quantification analysis (**F**), N(−) = N0, N(+) = N1 + N2; **, $P < 0.01$. **G,** Kaplan–Meier survival analysis showed that patients with HNSCC with higher CMTM6 expression had a shortened overall survival (cutoff = 95.05). Error bar, SD.

compared with control HNSCC tissues (Supplementary Table S1). Altogether, these data indicate that CMTM6 overexpression is associated with aggressive cancer and a poor prognosis for patients with HNSCC.

High CMTM6 expression is required for HNSCC proliferation

To further explore the role of CMTM6 in HNSCC, we investigated CMTM6 expression in a normal OKC line and a series of HNSCC cell lines (SCC4, SCC9, SCC15, SCC25, and CAL27) by Western blot analysis (**Fig. 2A**). The surface PD-L1 expression of these cell lines was analyzed by flow cytometry. CMTM6 and PD-L1 protein expression was higher in most cancer cells than in normal epithelial cells (**Fig. 2A** and **B**). Next, we used two shRNAs to construct CAL27 and SCC4 cells with stable, low CMTM6 expression; CMTM6 knockdown cells showed an approximately 80% reduction in CMTM6 protein expression compared with cells treated with a scrambled shRNA. CMTM6

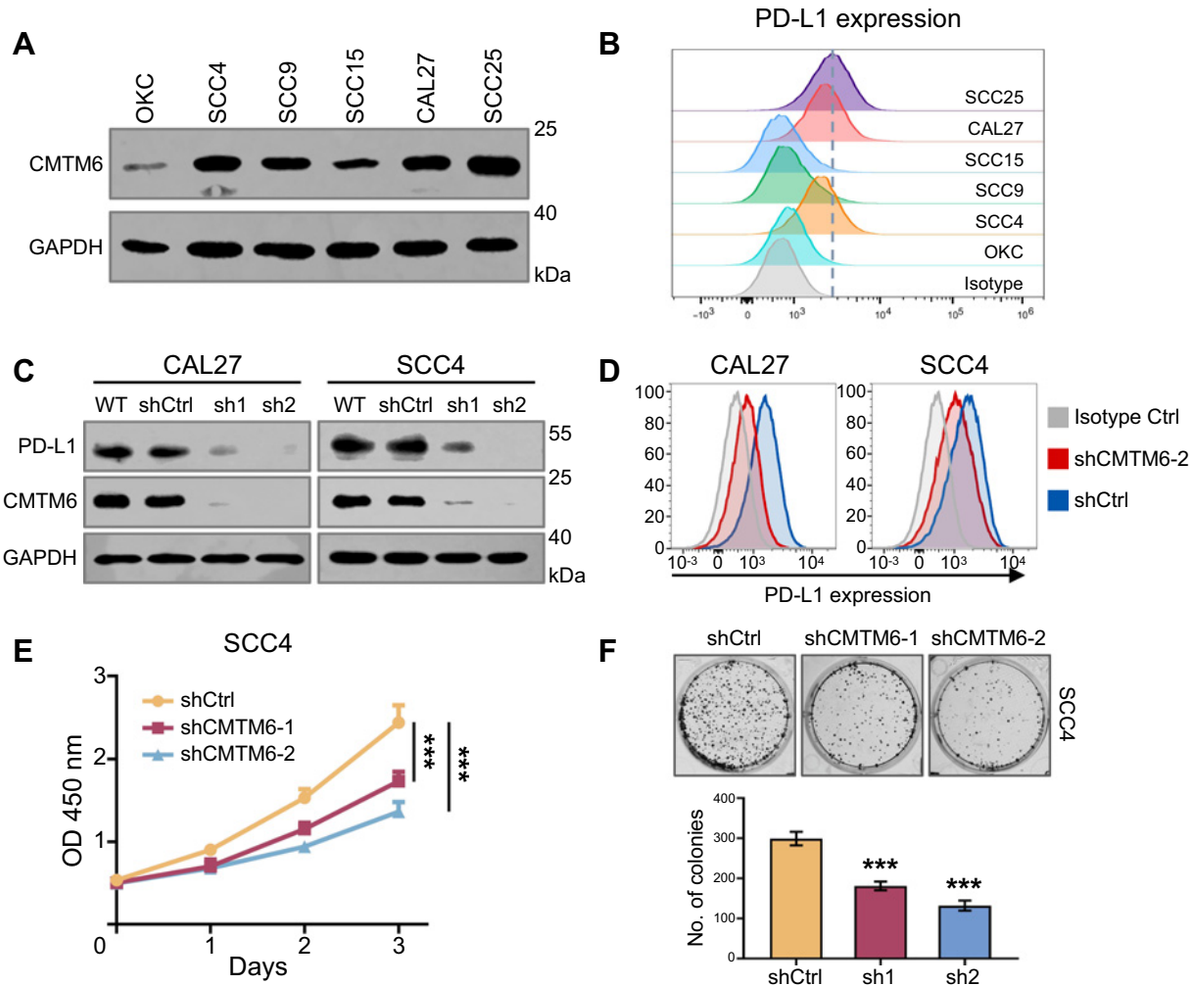

Figure 2.

Elevated CMTM6 expression in HNSCC cells promotes tumor growth. **A,** Western blot analysis of CMTM6 expression in five HNSCC cell lines and a normal OKC line. **B,** Flow cytometry analysis of cell surface PD-L1 in these cell lines. **C,** Western blot analysis of total CMTM6 and PD-L1 expression in CMTM6 knockdown or control CAL27 and SCC4 cells. **D,** Cell surface PD-L1 expression was reduced in CMTM6 knockout cells by flow cytometry analysis. **E,** Growth curves of CMTM6-depleted or control SCC4 cells as measured by a CCK-8 assay (***, $P < 0.001$). **F,** Representative images and quantitative analysis of anchorage-dependent colony formation assays in SCC4 cells (***, $P < 0.001$); error bar, SD. No., number. The data shown are representative of three experiments (**A–F**).

depletion decreased PD-L1 expression, as shown by immunoblotting and flow cytometry analyses (**Fig. 2C** and **D**). Tumor-intrinsic PD-L1 is involved in regulating tumor growth in cervical cancer, ovarian cancer, and melanoma (24, 25). Our studies revealed that CMTM6 knockout led to repression of the self-renewal and colony-forming capacities of SCC4 and CAL27 cells (**Fig. 2E** and **F**; Supplementary Fig. S2), perhaps explaining the finding that CMTM6 expression was associated with a high pathologic grade. Together, these findings suggest that CMTM6 may promote the proliferation of HNSCC cell lines.

CMTM6 depletion reduced nuclear translocation of β-catenin in HNSCC

The abovementioned results prompted us to further explore the mechanism of CMTM6 in HNSCC progression. Next, we analyzed most of the *CMTM6*-associated genes in the TCGA HNSCC cohort using the LinkedOmics database (26). As shown in the volcano plot, *CTNNB1* (gene encoding β-catenin) exhibited the highest positive correlation with *CMTM6* (**Fig. 3A**), and we observed a statistically significant correlation between *CMTM6* and *CTNNB1* by Spearman correlation analysis ($n = 520$, $P = 1.933\text{E-}47$, $R = 0.5768$; **Fig. 3B**). Numerous studies have shown that the Wnt/β-catenin signaling pathway plays roles in HNSCC tumorigenesis, and this pathway is involved in regulating tumor biological features, such as the maintenance of CSC phenotypes, proliferation, and EMT (7). Subsequently, we examined the relationship between CMTM6 and β-catenin with our HNSCC tissue microarray. The IHC staining results demonstrated that tumor regions with high CMTM6 expression contained abundant β-catenin (**Fig. 3C**). In contrast, β-catenin expression was reduced in tumor areas lacking CMTM6 (**Fig. 3C**). The positive correlation between CMTM6 and β-catenin expression was confirmed by analysis of protein ($n = 210$, $P < 0.0001$, $R = 0.5292$; **Fig. 3D**). To validate these findings, we performed immunofluorescence staining of CMTM6-knockout cells and control cells. CMTM6 depletion with shRNA

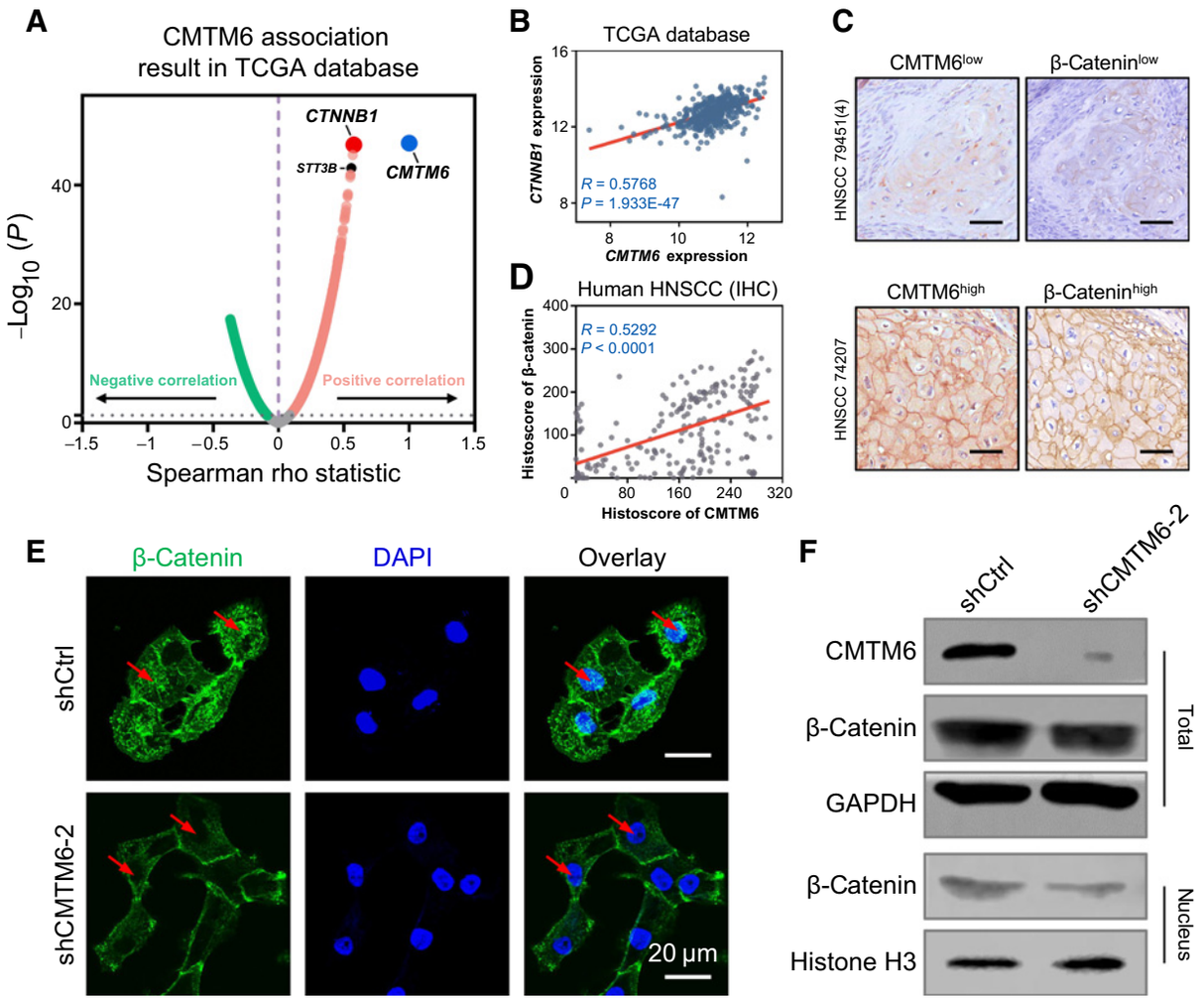

Figure 3.

CMTM6 expression has a positive correlation with the Wnt/β-catenin pathway in HNSCC. **A,** Volcano plot of *CMTM6*-associated genes by Spearman correlation coefficient test in the LinkedOmics database. The gray dashed line of $P = 0.05$ was plotted. **B,** Expression correlation between *CMTM6* and *CTNNB1* RNA expression in the TCGA HNSCC database. Correlation was analyzed using Spearman correlation coefficient test, $n = 520$. **C,** Representative IHC staining of CMTM6 and β-catenin in HNSCC specimens (scale bar, 50 μm). **D,** Pearson correlation analysis of CMTM6 and β-catenin protein expression in HNSCC tissue microarray ($n = 210$). **E,** The distribution of β-catenin (green) in CMTM6 knockdown and control CAL27 cells was analyzed by immunofluorescence (scale bar, 20 μm), and the red arrow indicates the location of the nucleus. **F,** Western blot analysis showed β-catenin expression levels in total or nuclear proteins of the control and CMTM6-silenced groups. The data shown are representative of three experiments (**E** and **F**).

lentivirus decreased β-catenin nuclear translocation (**Fig. 3E**). The Western blotting results showed that although total β-catenin was not significantly affected, nuclear β-catenin amounts were reduced in CMTM6-deficient cells compared with control cells (**Fig. 3F**). The above data indicate that CMTM6 may participate in the regulation of multiple biological characteristics of HNSCC by affecting the canonical Wnt/β-catenin signaling pathway.

Elevated CMTM6 sustains CSC phenotypes in HNSCC

Because the Wnt/β-catenin signaling pathway is involved in the functions of HNSCC CSCs (8), we determined whether CMTM6 plays a role in the acquisition of stem cell–like properties. Studies have shown that tumor spheres exhibit more CSC features than their adherent counterparts in HNSCC (27). The coimmunofluorescent staining of CMTM6 and several CSC markers (ALDH1, CD44 and BMI1; **Fig. 4A**; ref. 12) in HNSCC spheres indicated that CMTM6 was highly expressed in cells with strong stemness properties. This elevated expression of CMTM6 in spheres was validated by Western blotting (**Fig. 4B**). Enrichment of PD-L1 in $CD44^+$ CSCs may contribute to immune evasion by HNSCC (28). To investigate whether CMTM6 can directly affect the maintenance of CSCs, we measured ALDH activity in CMTM6-knockout cells and found that the percentages of $ALDH^{high}$ cells among CMTM6-depleted CAL27 and SCC4 cells were decreased (**Fig. 4C**). We then performed tumor sphere formation assays to evaluate the self-renewal ability of these two groups of cells. CMTM6-silenced cells formed fewer spheres (**Fig. 4D**). This finding was verified by immunofluorescence and Western blot analyses: the expression of several CSC-related markers was downregulated after CMTM6 depletion (**Fig. 4E** and **F**), indicating the role of CMTM6 in HNSCC cell self-renewal. To validate our results, we analyzed

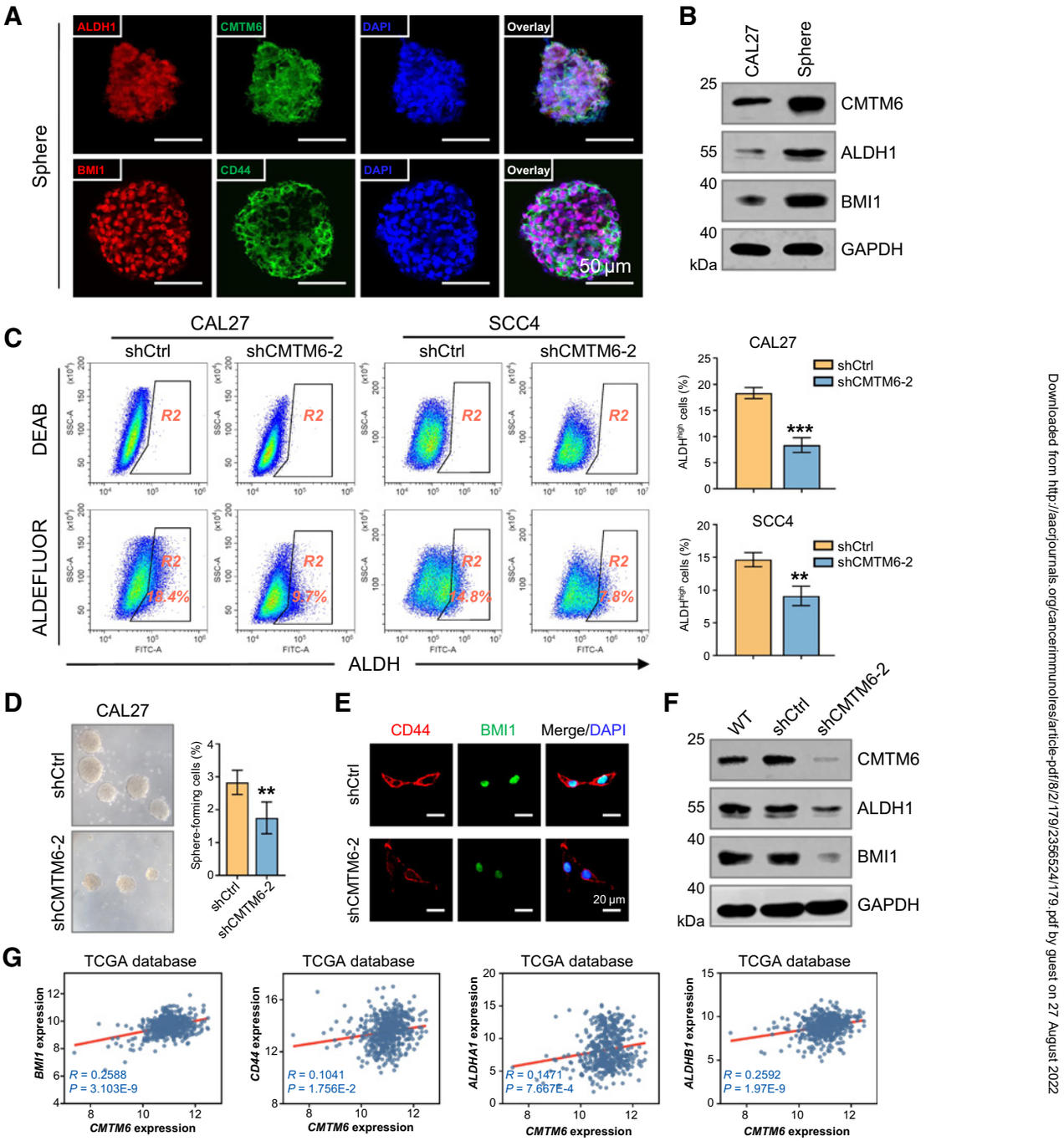

Figure 4.

CMTM6 is expressed in cancer stem cells and promotes stemness properties. **A,** Representative coimmunofluorescent staining images of CMTM6 (green) and CSC markers: ALDH1 (red), BMI1 (red), and CD44 (green) in tumorspheres (scale bar, 50 μm). **B,** The expression of CMTM6 and CSC-related proteins in spheres and adherent cells was detected by Western blotting. **C,** An ALDEFLUOR assay was conducted in CMTM6-deficient and control cells, and the percentage of $ALDH^{high}$ cells was quantified by flow cytometry (**, $P < 0.01$; ***, $P < 0.001$); error bar, SD. **D,** Representative images and quantitative analysis of a sphere formation assay (**, $P < 0.01$); error bar, SD. **E,** Immunofluorescence images show the expression of CSC markers BMI1 (green) and CD44 (red) after CMTM6 knockout (scale bar, 20 μm). **F,** Western blot results confirmed that CMTM6 knockout reduced the expression of CSC-related proteins. **G,** *CMTM6* was positively correlated with CSC genes in the TCGA HNSCC database using Spearman correlation coefficient test, $n = 520$. The data shown are representative of three experiments (**A–F**).

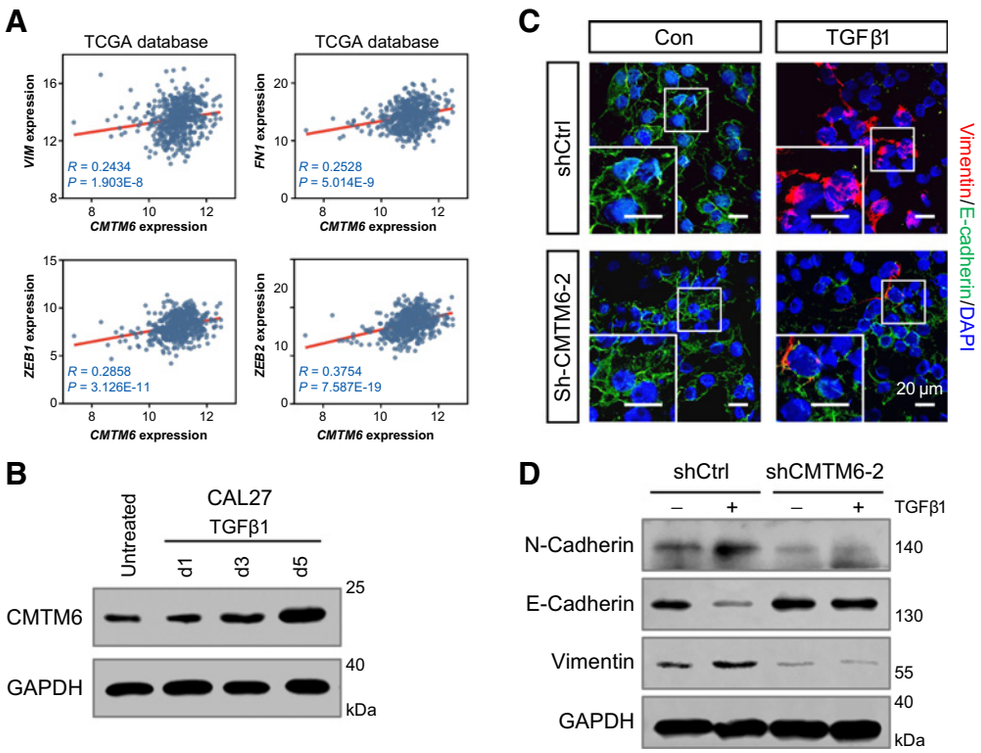

Figure 5.

Aberrant expression of CMTM6 is associated with EMT in HNSCC. **A,** Spearman correlation analysis of the public TCGA HNSCC database for the expression of *CMTM6* and mesenchymal (*VIM* and *FN1*) or EMT-TF genes (*ZEB1* and *ZEB2*), $n = 520$. **B,** Western blot analysis of CMTM6 in CAL27 cells undergoing TGFβ-induced EMT (8 ng/mL TGFβ1). **C,** Representative immunofluorescent staining images of E-cadherin (green) and Vimentin (red) in CMTM6 knockdown and control CAL27 cells treated with vehicle or 8 ng/mL TGFβ1 (36 hours; scale bar, 20 μm). **D,** Western blot analysis confirmed that CMTM6 depletion inhibited TGFβ-induced EMT in HNSCC (8 ng/mL TGFβ1, 36 hours). The data shown are representative of three experiments (**B–D**).

the association of *CMTM6* RNA expression with the expression of CSC-related genes (*CD44, ALDHA1, ALDH1B1*, and *BMI1*) in the TCGA HNSCC cohort. Expression of *CMTM6* and these CSC-related genes was positively correlated (**Fig. 4G**). Collectively, these data demonstrate that CMTM6 plays a role in acquisition of stem cell–like properties in HNSCC.

CMTM6 is involved in regulating EMT in HNSCC

Evidence suggests an association between EMT and the acquisition of CSC-like properties in various types of cancer (11), including HNSCC (12). TGFβ is an inducer of EMT that can also mediate PD-L1 induction (29), indicating that PD-L1 might play a role in modulating EMT. To investigate the connection between CMTM6 and EMT, we first analyzed the correlation between *CMTM6* and EMT-related genes in the TCGA HNSCC datasets. Indeed, *CMTM6* RNA amounts were significantly positively associated with the amounts of most mesenchymal markers (*VIM, FN1*, and *CDH2*) and EMT-TFs (*SNAIL, TWIST*, and *ZEB* family; **Fig. 5A**; Supplementary Fig. S3), with a particularly strong association with the *ZEB* family (**Fig. 5A**). In addition, cancer cell expression of PD-L1 is regulated by the miR-200/ZEB1 axis in non–small cell lung cancer (NSCLC) cells (30). These findings prompted us to determine whether CMTM6 is involved in regulating EMT in HNSCC; thus, we performed a TGFβ-induced EMT assay in HNSCC cells as described previously (31) and detected potential changes in CMTM6 expression. The immunoblotting results showed that CMTM6 expression gradually increased during EMT progression (**Fig. 5B**). When CMTM6 was knocked out in squamous cancer cells, the induction of EMT by TGFβ was inhibited. This finding was confirmed by both immunofluorescence and Western blot assays (**Fig. 5C** and **D**). Together, our observations suggest that CMTM6 may affect the induction of EMT in HNSCC.

Expression of CMTM6 correlated with immune checkpoint in human HNSCC

The PD-1/PD-L1 interaction leads to T-cell dysfunction and exhaustion, which helps tumor cells evade immune surveillance (32), and CMTM6 has been identified as a regulator of PD-L1 expression. Therefore, to determine whether CMTM6 also plays a role in T-cell tumor immunity in HNSCC, we analyzed its correlation with RNA expression of several immune checkpoint molecules in the TCGA HNSCC datasets. *CMTM6* expression was positively associated with expression of these genes, especially with *HAVCR2* (TIM-3; **Fig. 6A**; Supplementary Table S2). Our previous studies investigated the expression and function of certain immune checkpoints in HNSCC. To ascertain whether CMTM6 protein amounts are also associated with T-cell dysfunction, we conducted Pearson correlation analysis with CMTM6, PD-L1, LAG-3, TIM-3, VISTA, B7-H4, and B7-H3 expression in HNSCC tissues based on quantitative IHC results. Consistently, CMTM6 protein amounts were positively correlated with the amounts of these immune checkpoint markers (**Fig. 6B**).

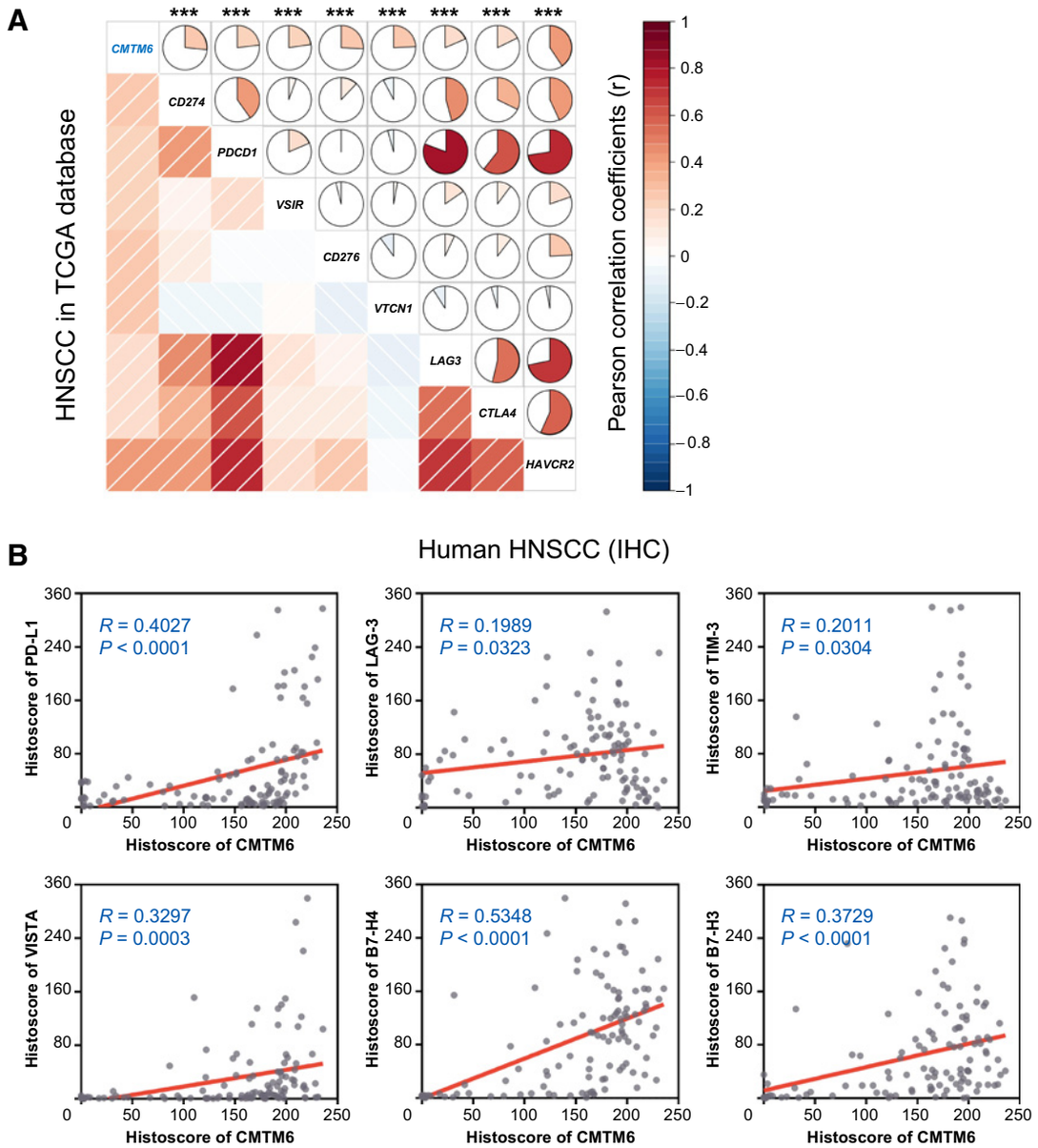

Figure 6.

Increased CMTM6 is correlated with immune checkpoint members in HNSCC. **A,** Expression correlation between *CMTM6* and immune checkpoint gene RNA amounts in the TCGA HNSCC database, $n = 520$, CMTM6 (*CMTM6*), PD-L1 (*CD274*), PD-1 (*PDCD1*), VISTA (*VSIR*), B7-H3 (*CD276*), B7-H4 (*VTCNI*), LAG-3 (*LAG3*), CTLA-4 (*CTLA4*), and TIM-3 (*HAVCR2*). **B,** Pearson correlation analysis of CMTM6 and several immune checkpoint expressions in human HNSCC tissue microarray based on the IHC results, $n = 116$.

Taken together, these results suggest that CMTM6 may play a role in T-cell suppression in HNSCC.

CMTM6 silencing inhibits tumor growth and enhances immune response in murine HNSCC

Studies have shown that targeting the upstream regulator of PD-L1 is an alternative strategy in melanoma (33). As a positive regulator of PD-L1 protein expression, can CMTM6 also amplify tumor-specific immunity? To address this question, we conducted an *in vivo* experiment with an immunocompetent HNSCC allograft mouse model (34, 35). Although PD-L1 expression is low in SCC7 cells, it was increased after stimulation with IFNγ, which was also increased in subcutaneously inoculated tumor tissue (**Fig. 7A** and **B**). Moreover, we verified that CMTM6 knockdown inhibited IFNγ-induced PD-L1 expression in SCC7 cells (**Fig. 7B**; Supplementary Fig. S4). Subsequently, wild-type, CMTM6-knockout, or scrambled shRNA SCC7 cells were injected subcutaneously into C3H/He mice. We then isolated SCC7 cells from the transplanted tumors at day 21 and performed flow cytometry to detect cell surface PD-L1 expression, which was lower in the CMTM6-depleted group (**Fig. 7C**). As

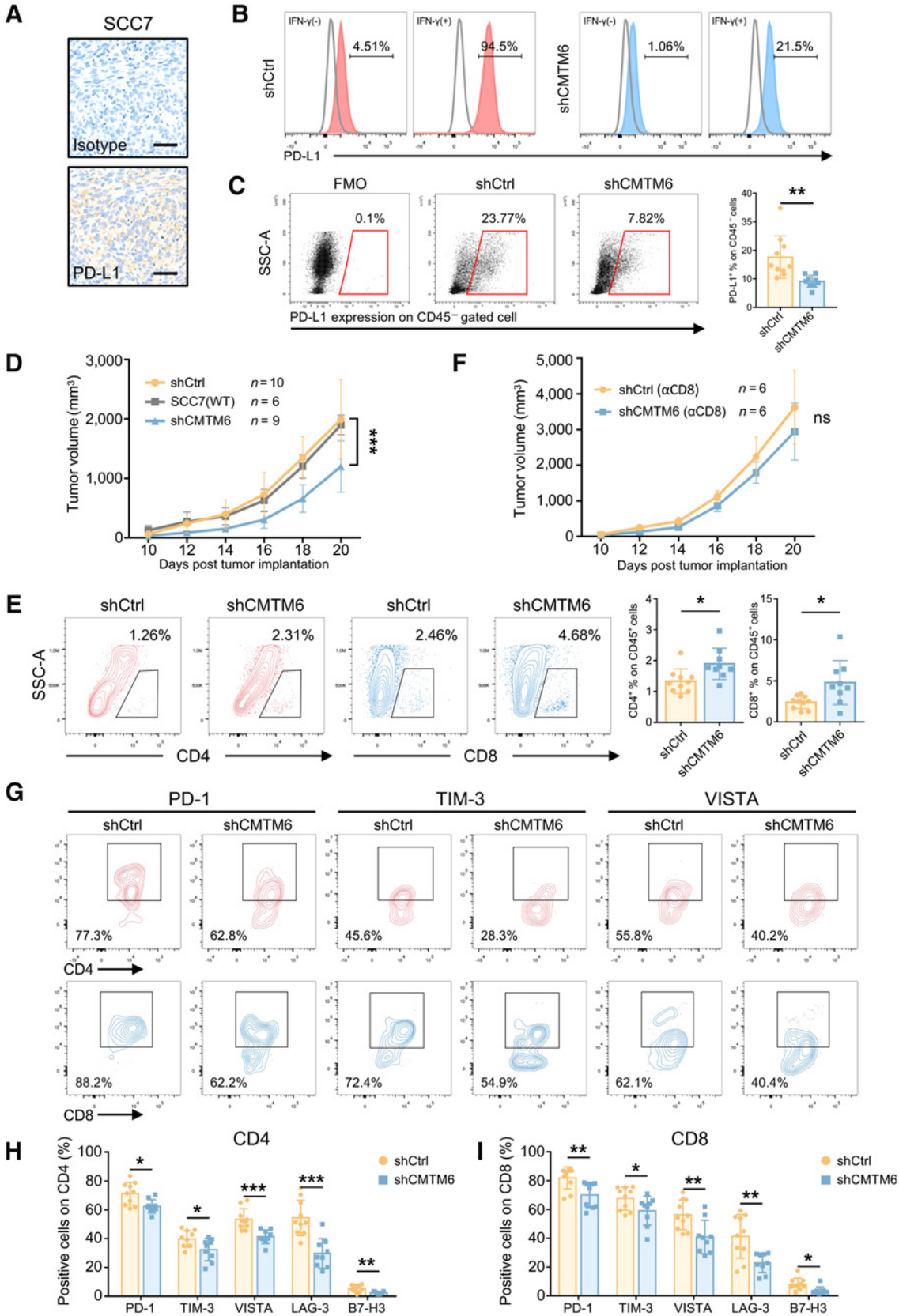

anticipated, the tumor growth of CMTM6-knockdown SCC7 cells was reduced compared with that of control cells (**Fig. 7D**). HNSCC tumors are immunosuppressive and characterized by impaired T-cell function and the accumulation of immunosuppressive cells (36). Therefore, we examined the effect of CMTM6 depletion on cancer immunity. The populations of $CD4^+$ and $CD8^+$ T cells in TILs were significantly elevated after CMTM6 silencing, as shown by flow cytometry and IHC assays (**Fig. 7E**; Supplementary Figs. S5 and S6A). To confirm that CMTM6 knockdown inhibits tumor growth in a manner dependent on T-cell activity, we used anti-$CD8^+$ to deplete $CD8^+$ cells. $CD8^+$ depletion significantly reduced the difference in tumor size between the two groups (**Fig. 7F**). Compared with the control group, the shCMTM6 group showed a significant decrease in the expression of the other five immune checkpoints in T cells, except for B7-H4 (**Fig. 7G–I**; Supplementary Fig. S6B and S6C). In addition, ELISA results showed that IFNγ, TNFα, and Granzyme B levels in tumor tissue were increased significantly in the CMTM6-depleted group (Supplementary Fig. S6D), suggesting T lymphocyte activation after CMTM6 knockout *in vivo*. Thus, these data reveal that CMTM6 depletion may improve antitumor immunity by increasing numbers of effector T cells in HNSCC.

Discussion

HNSCC is a heterogeneous tumor with high metastasis and recurrence rates, and there has been little improvement in 5-year survival over the past decades (6). EMT is part of the process of tumor metastasis (37), especially in squamous cell carcinoma (38). Briefly, cancer cells undergoing EMT lose their epithelial characteristics and gain mobility, which facilitates invasion and dissemination (9). Moreover, such cells are closely related to another small population of cells, CSCs, that may be tumor-initiating cells, the main culprits of tumor recurrence and chemotherapy resistance (11). In addition, CSC and EMT phenotypes may mediate tumor immunosuppression (13, 14); $CD44^+$ HNSCC cells can achieve immune escape by high PD-L1 expression (28), and a subset of TGFβ-responsive CSCs were reported to suppress T-cell antitumor immunity and drive tumor relapse by regulating CD80 expression in a squamous cell carcinoma mouse model (39). EMT induced by the EMT-TF Snail can promote tumor metastasis by accelerating immunosuppression (40). Upon Snail knockout in ovarian cancer cells, the number of $CD8^+$ T cells was increased; in contrast, the population of MDSCs among TILs was decreased (41). These findings revealed a relationship among EMT, CSCs, and tumor immunity that facilitates tumor progression. These findings prompted us to rethink the current therapeutic strategies for developing more effective treatments.

Immunotherapies based on immune checkpoints have emerged as a treatment option for various cancer types. Blockade of the PD-L1/PD-1 interaction with mAbs represents a milestone for anticancer immunotherapy. However, it is effective in only a small subset of patients (42). Therefore, it is necessary to explore alternative therapies or combined strategies to increase the drug response rate. Tumors expressing PD-L1 not only mediate immunosuppression but also have tumor-intrinsic functions in regulating EMT, CSC phenotypes, and drug resistance (15). For instance, PD-L1 promotes cell proliferation in cervical cancer (25), ovarian cancer, and melanoma (24); PD-L1 knockdown inhibits stem cell–like properties in breast cancer through the PI3K/AKT pathway (43). Moreover, EMT can induce PD-L1 accumulation on cancer cells through the miR-200/ZEB1 axis in NSCLC (30). In addition, PD-L1 is preferentially expressed on CSCs and facilitates CSC immune evasion in a STT3-dependent manner (29). Coincidentally, correlation analysis results showed that STT3 has a positive correlation with CMTM6 RNA expression. High PD-L1 expression on $CD44^+$ cells promotes a stronger immunosuppressive effect in HNSCC (28). This evidence suggests that we seek new therapeutic strategies besides antibody blockade. Currently, directly targeting the modulation of PD-L1 expression has yielded promising results in multiple myeloma (44). Ablation of *NRF2*, a gene upstream of PD-L1, enhanced tumor immunity in a melanoma mouse model (33). Because CMTM6 has been identified as a vital regulator of PD-L1, we speculated that CMTM6 may affect the above biological functions by modulating PD-L1 expression.

To verify this hypothesis, we first analyzed CMTM6 expression in HNSCC by IHC. CMTM6 was highly expressed in HNSCC, and its expression pattern was similar to that of PD-L1. In addition, patients with high CMTM6 expression had a poor prognosis, which was consistent with previous reports that PD-L1 is a poor prognostic predictor of HNSCC (45). Furthermore, CMTM6 was found to be enriched in high-grade HNSCC tumor samples, which suggested that CMTM6 overexpression is associated with tumor progression. Subsequently, we constructed stable CMTM6-knockout HNSCC cell lines and observed a decrease in PD-L1; moreover, cell proliferation was suppressed after CMTM6 depletion. This result is not contradictory to the finding that PD-L1 regulates tumor proliferation (15, 24, 25). Gene-wide correlation analysis based on the TCGA HNSCC database identified that *CTNNB1* was the gene most closely related to *CMTM6*. β-Catenin is part of the Wnt signaling pathway (46). Moreover, there is evidence that the Wnt/β-catenin pathway plays a role in regulating CSC/EMT phenotypes in HNSCC (7, 8), and activation of this pathway may prevent antitumor immunity in melanoma (47). The role of the Wnt pathway in tumor immunity is being discovered (48). Wnt signaling participates in the modulation of PD-L1 in triple-negative breast cancer, perhaps to help cancer cells escape immune surveillance (49). Our results indicate that CMTM6 can indeed affect the Wnt pathway. Thus, we investigated whether CMTM6 affects EMT and CSC phenotypes. As expected, CMTM6 knockdown inhibited stem cell–like properties and TGFβ-induced EMT to varying degrees. This finding suggested that CMTM6 possesses tumor-intrinsic functions analogous to those of PD-L1. CMTM6 has been reported to have synergistic correlations with multiple immune checkpoint inhibitors (19), and CMTM6 depletion enhanced the cytotoxic functions of T cells (17, 18). To investigate the relationship between CMTM6 and

Figure 7.

Targeting CMTM6 inhibits tumor growth in an immunocompetent HNSCC allograft mouse model. **A,** SCC7 tumor tissue sections were stained with PD-L1 antibody and IgG control. Scale bars, 50 μm. **B,** shCMTM6 and shCtrl SCC7 cells were cultured in the presence or absence of IFNγ (10 ng/mL) for 24 hours. The cells were stained with PD-L1 antibody and analyzed by flow cytometry. **C,** Cell surface PD-L1 expression on tumor cells after the allograft assay was detected by flow cytometry (tumor cells were gated by $CD45^-$; **, $P < 0.01$). **D,** Growth curve of SCC7 tumors (shCtrl, $n = 10$; WT, $n = 6$; shCMTM6, $n = 9$; ***, $P < 0.001$). **E,** $CD4^+$ and $CD8^+$ T cells in $CD45^+$ TILs were analyzed by flow cytometry (*, $P < 0.05$). **F,** Effects of $CD8^+$ T-cell depletion on the growth of CMTM6 knockdown or control SCC7 tumors ($n = 6$ mice per group). ns, not significant. **G,** Representative flow cytometry plots of PD-1^+, TIM-3^+, and VISTA$^+$ T-cell populations in control and CMTM6 knockdown SCC7 TILs. Quantification and statistical analysis results of PD-1^+, TIM-3^+, VISTA$^+$, LAG-3^+, and B7-H3^+ proportion in $CD4^+$ (**H**) and $CD8^+$ (**I**) T cells in two groups (*, $P < 0.05$; **, $P < 0.01$; and ***, $P < 0.001$). Error bar, SD. The data shown are representative of three (**A–C**) and two experiments (**D**).

immune checkpoints in HNSCC, we conducted Pearson correlation analysis with CMTM6 and other recognized immune checkpoints in the TCGA database and our HNSCC tissue microarrays. We observed positive correlations between CMTM6 and RNA and protein expression of the majority of immune checkpoint markers. Subsequently, we explored the potential of CMTM6 as an immunotherapy target using an immunocompetent HNSCC mouse model. Our results showed that knocking out CMTM6 not only inhibited tumor growth but also relieved the immunosuppressive state by increasing T-cell number and function; moreover, the expression of the immune checkpoint molecules PD-1, TIM-3, VISTA, LAG-3, and B7-H3 in TIL-T cells was decreased in the CMTM6 knockdown group, which was consistent with our previous TCGA and IHC correlation data. In addition, we noted that although not all HNSCC cell lines constitutively overexpress PD-L1, expression of this protein could be induced in the presence of IFNγ, indicating dynamic PD-L1 regulation in tumorigenesis. Treatment efficacy of PD-L1 antibody alone in SCC7 tumors was not satisfactory (50), and the reasons for this difference may be that CMTM6-regulated PD-L1 expression was not affected by IFNγ in the tumor microenvironment and that *CMTM6* gene knockout affected the intrinsic functions of tumor cells. In $CD8^+$ T-cell–depleted mice, the tumors in the shCMTM6 group were not significantly smaller than those in the control group, perhaps due to the slight PD-L1 expression in the SCC7 cell line and the weak CSC/EMT-related abilities.

In summary, we demonstrate that CMTM6 is overexpressed in HNSCC and is associated with positive lymph node status and high pathologic grade. Moreover, high CMTM6 expression indicates a poor prognosis. In addition, CMTM6 is highly correlated with the Wnt/β-catenin signaling pathway through which CMTM6 may affect the maintenance of CSCs and EMT phenotypes. We also explored the relationship between CMTM6 and tumor immunity. The correlation analysis results suggest a synergistic relationship between CMTM6 and immune checkpoint expression. *In vivo* experiments demonstrated that knocking out CMTM6 delays tumor growth, enhances T-cell function, and reduces the number of exhausted T cells. CMTM6 regulates PD-L1 independently of the IFN pathway. Therefore, compared with antibody blockade, targeting CMTM6 could actively inhibit the homeostatic feedback loop of IFN-induced PD-L1 expression in the tumor microenvironment. CMTM6 may be a useful immunotherapy, especially for patients with resistance to anti-PD-1/PD-L1 treatments. In addition, our study linked CSC/EMT phenotypes to tumor immunity. However, many problems remain to be solved, such as the lack of suitable drugs and an incomplete understanding of CMTM6 regulation in tumors. Nevertheless, CMTM6 may be a therapeutic target for the treatment of cancer.

Disclosure of Potential Conflicts of Interest

No potential conflicts of interest were disclosed.

Authors' Contributions

Conception and design: L. Chen, Z.-J. Sun
Development of methodology: L. Chen, Z.-J. Sun
Acquisition of data (provided animals, acquired and managed patients, provided facilities, etc.): L. Chen, Q.-C. Yang, L.-L. Yang, J.-F. Liu, H. Li, Z.-J. Sun
Analysis and interpretation of data (e.g., statistical analysis, biostatistics, computational analysis): L. Chen, Q.-C. Yang, L.-L. Yang, Y. Xiao, L.-L. Bu, Z.-J. Sun
Writing, review, and/or revision of the manuscript: L. Chen, W.-F. Zhang, Z.-J. Sun
Administrative, technical, or material support (i.e., reporting or organizing data, constructing databases): Y.-C. Li, W.-F. Zhang, Z.-J. Sun
Study supervision: W.-F. Zhang, Z.-J. Sun

Acknowledgments

This work was supported by National Natural Science Foundation of China (81874131, 81672668, and 81672667). The authors thank Shu-Yan Liang and Yin Liu from Wuhan Institute of Biotechnology for their excellent technical assistance on flow cytometry.

The costs of publication of this article were defrayed in part by the payment of page charges. This article must therefore be hereby marked *advertisement* in accordance with 18 U.S.C. Section 1734 solely to indicate this fact.

Received May 27, 2019; revised October 14, 2019; accepted November 22, 2019; published first November 26, 2019.

References

1. Ferlay J, Soerjomataram I, Dikshit R, Eser S, Mathers C, Rebelo M, et al. Cancer incidence and mortality worldwide: sources, methods and major patterns in GLOBOCAN 2012. Int J Cancer 2015;136:E359–86.
2. Puram SV, Rocco JW. Molecular aspects of head and neck cancer therapy. Hematol Oncol Clin North Am 2015;29:971–92.
3. Leemans CR, Braakhuis BJ, Brakenhoff RH. The molecular biology of head and neck cancer. Nat Rev Cancer 2011;11:9–22.
4. Leemans CR, Snijders PJF, Brakenhoff RH. The molecular landscape of head and neck cancer. Nat Rev Cancer 2018;18:269–82.
5. Castellsague X, Alemany L, Quer M, Halec G, Quiros B, Tous S, et al. HPV involvement in head and neck cancers: comprehensive assessment of biomarkers in 3680 patients. J Natl Cancer Inst 2016;108:djv403.
6. Chi AC, Day TA, Neville BW. Oral cavity and oropharyngeal squamous cell carcinoma–an update. CA A Cancer J Clin 2015;65:401–21.
7. Lee SH, Koo BS, Kim JM, Huang S, Rho YS, Bae WJ, et al. Wnt/β-catenin signalling maintains self-renewal and tumourigenicity of head and neck squamous cell carcinoma stem-like cells by activating Oct4. J Pathol 2014;234:99–107.
8. Alamoud KA, Kukuruzinska MA.Emerging insights into Wnt/beta-catenin signaling in head and neck cancer. J Dent Res 2018;97:665–73.
9. Pastushenko I, Brisebarre A, Sifrim A, Fioramonti M, Revenco T, Boumahdi S, et al. Identification of the tumour transition states occurring during EMT. Nature 2018;556:463–8.
10. Brabletz T, Kalluri R, Nieto MA, Weinberg RA. EMT in cancer. Nat Rev Canc 2018;18:128–34.
11. Shibue T, Weinberg RA. EMT, CSCs, and drug resistance: the mechanistic link and clinical implications. Nat Rev Clin Oncol 2017;14:611–29.
12. Chen C, Zimmermann M, Tinhofer I, Kaufmann AM, Albers AE. Epithelial-to-mesenchymal transition and cancer stem(-like) cells in head and neck squamous cell carcinoma. Cancer Lett 2013;338:47–56.
13. Terry S, Savagner P, Ortiz-Cuaran S, Mahjoubi L, Saintigny P, Thiery JP, et al. New insights into the role of EMT in tumor immune escape. Mol Oncol 2017;11:824–46.
14. Zhang D, Tang DG, Rycaj K. Cancer stem cells: Regulation programs, immunological properties and immunotherapy. Semin Cancer Biol 2018;52:94–106.
15. Dong P, Xiong Y, Yue J, Hanley SJB, Watari H. Tumor-intrinsic PD-L1 signaling in cancer initiation, development and treatment: beyond immune evasion. Front Oncol 2018;8:386.
16. Han W, Ding P, Xu M, Wang L, Rui M, Shi S, et al. Identification of eight genes encoding chemokine-like factor superfamily members 1-8 (CKLFSF1-8) by in silico cloning and experimental validation. Genomics 2003;81:609–17.
17. Mezzadra R, Sun C, Jae LT, Gomez-Eerland R, de Vries E, Wu W, et al. Identification of CMTM6 and CMTM4 as PD-L1 protein regulators. Nature 2017;549:106–10.
18. Burr ML, Sparbier CE, Chan YC, Williamson JC, Woods K, Beavis PA, et al. CMTM6 maintains the expression of PD-L1 and regulates anti-tumour immunity. Nature 2017;549:101–5.
19. Guan X, Zhang C, Zhao J, Sun G, Song Q, Jia W. CMTM6 overexpression is associated with molecular and clinical characteristics of malignancy and predicts poor prognosis in gliomas. EBioMedicine 2018;35:223–43.

20. Mamessier E, Birnbaum DJ, Finetti P, Birnbaum D, Bertucci F. CMTM6 stabilizes PD-L1 expression and refines its prognostic value in tumors. Ann Transl Med 2018;6:54.
21. Sun ZJ, Zhang L, Hall B, Bian Y, Gutkind JS, Kulkarni AB. Chemopreventive and chemotherapeutic actions of mTOR inhibitor in genetically defined head and neck squamous cell carcinoma mouse model. Clin Cancer Res 2012;18: 5304–13.
22. Chandrashekar DS, Bashel B, Balasubramanya SAH, Creighton CJ, Ponce-Rodriguez I, Chakravarthi B, et al. UALCAN: a portal for facilitating tumor subgroup gene expression and survival analyses. Neoplasia 2017;19:649–58.
23. Budczies J, Klauschen F, Sinn BV, Gyorffy B, Schmitt WD, Darb-Esfahani S, et al. Cutoff finder: a comprehensive and straightforward Web application enabling rapid biomarker cutoff optimization. PLoS ONE 2012;7:e51862.
24. Clark CA, Gupta HB, Sareddy G, Pandeswara S, Lao S, Yuan B, et al. Tumor-intrinsic PD-L1 signals regulate cell growth, pathogenesis, and autophagy in ovarian cancer and melanoma. Cancer Res 2016;76:6964–74.
25. Dong P, Xiong Y, Yu J, Chen L, Tao T, Yi S, et al. Control of PD-L1 expression by miR-140/142/340/383 and oncogenic activation of the OCT4-miR-18a pathway in cervical cancer. Oncogene 2018;37:5257–68.
26. Vasaikar SV, Straub P, Wang J, Zhang B. LinkedOmics: analyzing multi-omics data within and across 32 cancer types. Nucleic Acids Res 2018;46:D956–D63.
27. Yan M, Yang X, Wang L, Clark D, Zuo H, Ye D, et al. Plasma membrane proteomics of tumor spheres identify CD166 as a novel marker for cancer stem-like cells in head and neck squamous cell carcinoma. Mol Cell Proteomics 2013; 12:3271–84.
28. Lee Y, Shin JH, Longmire M, Wang H, Kohrt HE, Chang HY, et al. CD44+ cells in head and neck squamous cell carcinoma suppress T-Cell-mediated immunity by selective constitutive and inducible expression of PD-L1. Clin Cancer Res 2016;22:3571–81.
29. Hsu JM, Xia W, Hsu YH, Chan LC, Yu WH, Cha JH, et al. STT3-dependent PD-L1 accumulation on cancer stem cells promotes immune evasion. Nat Commun 2018;9:1908.
30. Chen L, Gibbons DL, Goswami S, Cortez MA, Ahn YH, Byers LA, et al. Metastasis is regulated via microRNA-200/ZEB1 axis control of tumour cell PD-L1 expression and intratumoral immunosuppression. Nat Commun 2014;5: 5241.
31. Chen L, Li YC, Wu L, Yu GT, Zhang WF, Huang CF, et al. TRAF6 regulates tumour metastasis through EMT and CSC phenotypes in head and neck squamous cell carcinoma. J Cell Mol Med 2018;22:1337–49.
32. Boussiotis VA. Molecular and biochemical aspects of the PD-1 checkpoint pathway. N Engl J Med 2016;375:1767–78.
33. Zhu B, Tang L, Chen S, Yin C, Peng S, Li X, et al. Targeting the upstream transcriptional activator of PD-L1 as an alternative strategy in melanoma therapy. Oncogene 2018;37:4941–54.
34. Rossa CJ, D'Silva NJ. Immune-relevant aspects of murine models of head and neck cancer. Oncogene 2019;38:3973–88.
35. O'Malley BW, Cope KA, Johnson CS, Schwartz MR. A new immunocompetent murine model for oral cancer. Arch Otolaryngol Head Neck Surg 1997;123:20–4.
36. Ferris RL. Immunology and immunotherapy of head and neck cancer. J Clin Oncol 2015;33:3293–304.
37. Lambert AW, Pattabiraman DR, Weinberg RA. Emerging biological principles of metastasis. Cell 2017;168:670–91.
38. Tsai JH, Donaher J, Murphy D, Chau S, Yang J. Spatiotemporal regulation of epithelial-mesenchymal transition is essential for squamous cell carcinoma metastasis. Cancer cell 2012;22:725–36.
39. Miao Y, Yang H, Levorse J, Yuan S, Polak L, Sribour M, et al. Adaptive immune resistance emerges from tumor-initiating stem cells. Cell 2019;177:1172–86.
40. Kudo-Saito C, Shirako H, Takeuchi T, Kawakami Y. Cancer metastasis is accelerated through immunosuppression during Snail-induced EMT of cancer cells. Cancer Cell 2009;15:195–206.
41. Taki M, Abiko K, Baba T, Hamanishi J, Yamaguchi K, Murakami R, et al. Snail promotes ovarian cancer progression by recruiting myeloid-derived suppressor cells via CXCR2 ligand upregulation. Nat Commun 2018;9:1685.
42. Ribas A, Wolchok JD. Cancer immunotherapy using checkpoint blockade. Science 2018;359:1350–5.
43. Almozyan S, Colak D, Mansour F, Alaiya A, Al-Harazi O, Qattan A, et al. PD-L1 promotes OCT4 and Nanog expression in breast cancer stem cells by sustaining PI3K/AKT pathway activation. Int J Cancer 2017;141:1402–12.
44. Tremblay-LeMay R, Rastgoo N, Chang H. Modulating PD-L1 expression in multiple myeloma: an alternative strategy to target the PD-1/PD-L1 pathway. J Hematol Oncol 2018;11:46.
45. Lin YM, Sung WW, Hsieh MJ, Tsai SC, Lai HW, Yang SM, et al. High PD-L1 expression correlates with metastasis and poor prognosis in oral squamous cell carcinoma. PLoS ONE 2015;10:e0142656.
46. Clevers H, Loh KM, Nusse R. Stem cell signaling. An integral program for tissue renewal and regeneration: Wnt signaling and stem cell control. Science 2014;346: 1248012.
47. Spranger S, Bao R, Gajewski TF. Melanoma-intrinsic β-catenin signalling prevents anti-tumour immunity. Nature 2015;523:231–5.
48. Staal FJ, Luis TC, Tiemessen MM. WNT signalling in the immune system: WNT is spreading its wings. Nat Rev Immunol 2008;8:581–93.
49. Castagnoli L, Cancila V, Cordoba-Romero SL, Faraci S, Talarico G, Belmonte B, et al. WNT signaling modulates PD-L1 expression in the stem cell compartment of triple-negative breast cancer. Oncogene 2019;38:4047–60.
50. Kang S, Keam B, Ahn Y, Park H, Kim M, Kim TM, et al. Inhibition of MEK with trametinib enhances the efficacy of anti-PD-L1 inhibitor by regulating anti-tumor immunity in head and neck squamous cell carcinoma. Oncoimmunology 2019;8:e1515057.